Published in final edited form as:
Nat Microbiol. 2020 December 01; 5(12): 1481–1489. doi:10.1038/s41564-020-00797-5.

Symbiosis, virulence and natural products biosynthesis in entomopathogenic bacteria are regulated by a small RNA

Nick Neubacher[1,*], **Nicholas J. Tobias**[1,2,3,*], **Michaela Huber**[4,5,6,*], **Xiaofeng Cai**[1], **Timo Glatter**[7], **Sacha J. Pidot**[8], **Timothy P. Stinear**[8], **Anna Lena Lütticke**[1], **Kai Papenfort**[4,5], **Helge B. Bode**[1,2,3,9,#]

[1]Molekulare Biotechnologie, Fachbereich Biowissenschaften, Goethe-Universität Frankfurt, Frankfurt am Main, Germany

[2]LOEWE Center for Translational Biodiversity in Genomics (TBG), Germany

[3]Senckenberg Gesellschaft für Naturforschung, Frankfurt am Main, Germany

[4]Friedrich Schiller University, Institute of Microbiology, 07745 Jena, Germany

[5]Microverse Cluster, Friedrich Schiller University Jena, 07743 Jena, Germany

[6]Ludwig-Maximilians-University of Munich, Faculty of Biology I, 82152 Martinsried, Germany

[7]Core Facility for Mass Spectrometry and Proteomics, Max Planck Institute for Terrestrial Microbiology, Marburg, Germany

[8]Department of Microbiology and Immunology, Peter Doherty Institute for Infection and Immunity, University of Melbourne, Melbourne, Australia

[9]Buchmann Institute for Molecular Life Sciences, Goethe-Universität Frankfurt, Frankfurt am Main, Germany

Abstract

Photorhabdus and *Xenorhabdus* species have mutualistic associations with nematodes and an entomopathogenic stage[1,2] in their lifecycles. In both stages numerous specialized metabolites are produced that have roles in symbiosis and virulence[3,4]. Although regulators have been implicated in the regulation of these specialized metabolites[3,4], how small regulatory RNAs (sRNAs) are involved in this process is not clear. We show here that the Hfq-dependent sRNA, ArcZ, is required for specialized metabolite production in *Photorhabdus* and *Xenorhabdus*. We discovered that ArcZ directly base-pairs with the mRNA encoding HexA, which represses the expression of specialized metabolite gene clusters. In addition to specialized metabolite genes, we show that the

[#]Corresponding author h.bode@bio.uni-frankfurt.de.
[*]Co-first authors

Contributions

These authors contributed equally: Nick Neubacher, Nicholas J. Tobias, Michaela Huber.
N.N., N.J.T., M.H., X.C., A.L., T.G. and S.J.P. performed experiments except sequencing of the transposon insertion mutants, which was performed by S.J.P., and T.P.S. N.N., N.J.T., M.H., K.P. and H.B.B. designed the study, discussed the results and commented on the manuscript. N.N., N.J.T. and M.H. analyzed and interpreted the data. N.N., N.J.T. and M.H. wrote the manuscript. All authors read and approved the final manuscript.

Competing interests

The authors declare no competing interests.

Europe PMC Funders Author Manuscripts

ArcZ regulon affects ~15% of all transcripts in *Photorhabdus* and *Xenorhabdus*. Thus, the ArcZ sRNA is crucial for specialized metabolite production in *Photorhabdus* and *Xenorhabdus* species and might well become a useful tool for metabolic engineering and identification of commercially relevant natural products.

Regulation via *trans*-encoded sRNAs typically occurs by imperfect base-pairing of sRNAs with their mRNA targets and can be mediated by RNA chaperones such as Hfq and ProQ[13,14]. RNA duplex formation is usually short (6 to 12 nucleotides) and can result in conformational changes in RNA secondary structure with various regulatory outcomes[5]. The RNA chaperone Hfq is highly conserved throughout the bacterial kingdom[6]. Several complex phenotypes have been attributed to Hfq with its regulatory roles being achieved by stabilizing sRNAs and/or mRNAs, mediating base-pairing of sRNAs and their targets, modulation of mRNA translation[6], as well as accelerating the degradation of sRNAs and their targets[7]. Expression of sRNAs is highly dynamic, with sRNA profiles in *Salmonella* shown to be strongly dependent on the bacterial growth phase[8]. ArcZ is one of the few Hfq-bound sRNAs whose expression remains relatively constant in *Salmonella* throughout the growth phases, making up ~7-12% of all reads identified by Hfq co-immunoprecipitation experiments[8]. ArcZ is transcribed as a 129 nt primary transcript (Figure 1a) and processed into a stable short form (~50 nt)[8–10]. The processed short form of ArcZ directly activates *rpoS* translation and inhibits the expression of several other genes[10,11]. In *E. coli*, the expression of *arcZ* is repressed by the ArcA-ArcB two-component system under anaerobic conditions. In a negative feedback loop, *arcZ* represses, and is repressed by *arcB* transcription[10]. Although there is a wealth of research on ArcZ in *E. coli* and *Salmonella* [8–10], its function in other bacteria remains unclear.

SM in bacteria are often responsible for ecologically important activities[12]. In the case of *Xenorhabdus* and *Photorhabdus*, SMs play an essential role in cross-kingdom interactions with nematodes, various insects, as well as bacterial and fungal species competing for the same food source[13]. Our earlier work on *Photorhabdus* showed that deletion of *hfq* resulted in severe perturbation of gene networks, including several key regulators[4]. This led to an overall decrease in SM production and a failure of the bacteria to support their obligate symbiosis with nematodes. Despite SMs playing a central role in the life cycle of the symbiosis, the exact ecological function for many of these compounds remained unknown. Over the past years, significant advances have been made towards finding bioactivities for many of the SMs, with assigned functions including cell-cell communication (photopyrones, dialkylresorcinols[14,15]), nematode development (isopropylstilbene[16]), defense against food-competitors (isopropylstilbene, rhabdopeptides[16,17]), or insect pathogenicity (rhabduscin, rhabdopeptides, glidobactin[17–19]). However, understanding the full potential of SMs in these bacteria is still hampered by a somewhat limited understanding of when individual SMs are produced, and their regulation in general. Regulation of SM in *Photorhabdus* and *Xenorhabdus* so far implicated the regulators Hfq, HexA (also LrhA), LeuO and Lrp[3,4,20,21]. Deletion of *hfq* in *Photorhabdus* resulted in complex regulatory changes, including a strong up-regulation of HexA, a known repressor of SM production[4]. Consequently, SM production was completely abolished in this strain and nematode development was severely restricted.

Europe PMC Funders Author Manuscripts

Given the overlapping lifecycles and niche occupation, we hypothesized that deletion of *hfq* in *Xenorhabdus* would have a similar effect on the production of SMs and the transcriptome. We confirmed this in *X. szentirmaii* DSM16338 using both high-performance LCMS/MS and RNA-seq (Supplementary Note 1, Supplementary Table 1). To further elucidate the mechanism of SM regulation, we investigated Hfq binding partners. To this end, we sequenced both *X. szentirmaii* and *P. laumondii* using a sRNA sequencing protocol and combined this with CappableSeq data to globally annotate transcriptional start sites belonging to coding sequences or potential previously undescribed sRNAs (Supplementary Note 2, Supplementary Table 2). We confirmed expression of several of these sRNAs by Northern blot analysis (Extended Data Figures 1 & 2). To identify RNA-protein interactions on a global scale, we next employed RNA immunoprecipitation followed by high-throughput sequencing (RIPseq) using chromosomally produced Hfq:3xFLAG protein as bait. We performed these experiments at two different cell densities (*i.e.* OD_{600} 0.5 and OD_{600} 5.0, for a full list of ODs from different experiments, see Supplementary Table 3). From the corresponding sequencing data, we first identified regions of 5 bp or more that were enriched in our tagged Hfq strain (see Methods). We then searched for sRNAs that were specifically enriched in the tagged samples, when compared to the untagged samples. We identified a total of 37 binding sites in annotated sRNAs (35 unique sRNAs) at OD_{600} 0.5 and 37 binding sites (34 unique) at OD_{600} 5.0 that were enriched by at least three-fold in both replicates (Figure 1b, Supplementary Table 4). During early exponential growth, 11 sRNAs (out of 35) were identified that are described to associate with Hfq in other species, while 10 (out of 34) are known from those that were enriched at OD_{600} 5.0. As a second step, we examined mRNAs enriched in the data. At OD 5.0, 402 mRNAs and 32 annotated 5'-UTRs were identified to associate with Hfq. At OD 0.5 a total of 1,003 mRNAs and 29 5'-UTRs were detected (Figure 1c, Supplementary Table 5).

We hypothesized that the performed Hfq RIP-seq analysis would allow us to identify key sRNAs involved in SM repression. However, our analysis identified >50 potential sRNAs binding Hfq (across both ODs, Figure 1b). Therefore, rather than individually deleting each sRNA, we constructed a transposon mutant library using pSAM-BT_Kan (see Methods and Supplementary Note 3) and searched for phenotypes consistent with that of the Δ*hfq* strain. The red color afforded to the bacteria by anthraquinone (AQ) production makes the strain especially suitable for transposon mutagenesis when screening for mutants defective in SM biosynthesis. We screened approximately 60,000 clones for obvious phenotypic alterations. Several mutants were defective in some facets of SM production and showed growth defects (Supplementary Note 3, Extended Data Figure 3, Supplementary Table 6), however, only one displayed the desired phenotype. Re-sequencing of this strain followed by read mapping revealed that the transposon was inserted within an intergenic region associated with the *arcZ* sRNA gene (Supplementary Figure 1).

ArcZ is a well-known Hfq-associated sRNA, which also appeared in our list of Hfq-bound sRNAs in *P. laumondii* (Figure 1b, Supplementary Table 4). To verify that the observed phenotype was derived from the transposon-insertion, we generated a Δ*arcZ* mutant by deleting the major part of the sRNA (Supplementary Figure 1) and a complemented strain by reintroducing an intact version of *arcZ* at the original locus. Northern blot analysis was performed to verify the absence of ArcZ in the deletion mutant and the presence of ArcZ in

the WT and the complementation mutant (Figure 2a). RNA sequencing of Δ*arcZ* mutant showed severe transcriptomic changes compared to the WT and Δ*arcZ::arcZ* mutant of *P. laumondii*, reminiscent of that seen in *P. laumondii* Δ*hfq* (Supplementary Note 4, Supplementary Tables 7 & 8, Supplementary Figure 2). SM production titers in the Δ*arcZ* strain were strongly decreased, similar to that seen in the transposon-insertion mutant and the complementation strain restored SM production (Figure 2c-h).

To corroborate the role of ArcZ in SM production, ArcZ mRNA targets were predicted using CopraRNA[22] (Supplementary Tables 9 & 10). One hit, warranting further investigation was *hexA* (*lrhA*), which was previously identified as a highly upregulated gene in our strains and which represses SM production in both *P. laumondii* [23] and *Xenorhabdus* [3]. CopraRNA predicted a 9 bp-long RNA duplex involving the 5'-UTR of *hexA* and the processed isoform of ArcZ (Figure 3a). This base-pairing is reminiscent of previously reported ArcZ targets in other bacteria requiring RNase E-mediated release of the sRNA's seed region[11]. We also identified a corresponding enriched RNA sequence upstream of the *hexA* CDS at OD_{600} 0.5 in the RIPseq experiments (Figure 1c, Supplementary Figure 3). We hypothesized that, through Hfq, ArcZ might bind to the *hexA* transcript leading to repression of HexA. In lab cultures, where SMs are produced, we hypothesized that Hfq and ArcZ prevent HexA production, allowing the strain to synthesize SM. However, if either *hfq* or *arcZ* were deleted, we would expect that *hexA* is no longer repressed, resulting in severely reduced SM production. To test this idea, we altered the predicted site of the ArcZ-*hexA* interaction to a *Pac*I restriction site (TTAATTAA) and created a knock-in of *hexA* with the modified sequence in a Δ*hexA* strain (Supplementary Figure 4a & b). We predicted that a knock-in of *hexA* with an altered 5'-UTR would result in a failure of ArcZ to bind, leading to reduced SM titers. Indeed, the SM production titers in the knock-in mutant with the altered binding site upstream of *hexA* were greatly reduced (Figure 2c-h).

To verify the proposed interaction region, we conducted a compensatory base mutation study in *E. coli*. The fifth base-pair of the proposed interaction region was exchanged in the *arcZ* sequence, the *hexA* 5'UTR, or both by site directed mutagenesis (Figure 3a). The *hexA* 5' UTR sequence was fused to *gfp*. The GFP output was measured to determine the efficiency of inhibition (Figure 3b & c). For the control, the GFP signal derived from the expression of *hexA*::*gfp* was measured and set to 1. When p-*arcZ* was expressed together with *hexA*::*gfp*, HexA repression was increased 32-fold compared to the control. Additionally, when p-*arcZ** (G79C) was expressed, ArcZ* was no longer able to repress HexA. For *hexA**::*gfp* (C-46G) in combination with the native ArcZ, HexA repression was only slightly increased compared to the control, suggesting that ArcZ can still bind to the 5' UTR of *hexA* but with a much reduced efficiency. When combining p-*arcZ** (G79C) with *hexA**::*gfp* (C-46G), HexA::GFP repression was increased 39-fold, which confirms our hypothesis that ArcZ binds to the 5'-UTR of *hexA* to repress HexA production. Of note, this base-pairing sequence is located ~50 nts upstream of the *hexA* translational start site (Fig. 3a) and thus ArcZ binding is unlikely to compete with recognition of the mRNA by 30S ribosomes[24]. Instead, alignment of the *P. laumondii hexA* 5' UTR revealed that the ArcZ binding site is CA-rich and highly conserved among other SM-producing bacteria (Supplementary Figure 5). CA-rich sequences located in proximity to translation initiation sites are well-known translational enhancers and sequestration of these regulatory elements by sRNAs has been reported to

down-regulate gene expression[25,26], which might also be relevant for the ArcZ-*hexA* interaction reported here. In addition, we conducted a proteomic analysis with the WT, Δ*arcZ*, Δ*hfq* and Δ*hexA*::*hexA*_PacI_UTR strains of *P. laumondii*. We used a label free quantification of quadruplicate samples to determine the HexA abundancy in each strain. HexA levels were significantly elevated in all mutant strains (11.8 to 22.7 fold, Supplementary Table 11) compared to the WT, further supporting this mechanism of regulation for SM production.

The *arcZ* gene and its genomic organization are highly conserved among enterobacterial species[9] (Figure 1a). Since the control of SMs in *Photorhabdus* relays a fundamental ability for these bacteria to occupy their specific niche, we investigated the possibility that the same mechanism occurs in the closely related *Xenorhabdus*. Given the SM reduction in *X. szentirmaii* Δ*hfq*, we constructed a Δ*arcZ* mutant in *X. szentirmaii* in a similar fashion to *P. laumondii,* by deleting 90bp of the predicted *arcZ* sequence. We verified via Northern blots that ArcZ was no longer produced by the deletion mutant and that complementation of the deletion led to production of ArcZ again (Figure 3d). Subsequently, we investigated the transcriptome and SM profile of the WT, deletion and complementation mutant. (Figure 3e, Supplementary Table 12). Consistent with *P. laumondii,* deletion of *arcZ* resulted in a global effect on the transcriptome as well as severely reduced SM titers, both of which was complemented in the Δ*arcZ*::*arcZ* complementation mutant (Figure 3e, Figure 4).

Our results highlight the critical role of ArcZ in regulating specialized metabolism in these strains. In fact, the critical nature of SM from *Photorhabdus* and *Xenorhabdus* in modulating the insect immune response indicated that ArcZ might be required for niche occupation by these bacteria. In the *P. laumondii* Δ*arcZ* strain, we observed an inability to support nematode development (Extended Data Figure 4), consistent with our earlier observations in the Δ*hfq* mutant[4]. However, the same was not seen in *X. szentirmaii*. We suspect this might be because of the observed increase in protoporphyrin IX (PPIX) production in the *X. szentirmaii* Δ*arcZ* strain (Supplementary Note 5). PPIX is a precursor of heme, which is an important cofactor for key biological processes such as oxidative metabolism[27], protein translation[28], maintaining protein stability[29] and many others. However, PPIX cannot be synthesized *de novo* by *Caenorhabditis elegans* and other nematodes[30]. The nematodes therefore rely on external PPIX sources (such as from symbiotic bacteria), which positively affects their growth, reproduction and development[31]. It is interesting that despite *P. laumondii* also being capable of producing PPIX, the *Heterorhabditis* nematode reproduction was not supported in either the Δ*arcZ* mutant, nor the Δ*hfq* strain. This is possibly indicative of the nematode specific requirements for reproduction, which may also include isopropylstilbene as an essential factor in *Heterorhabditis* [16], where no analogous compound is yet known to be required for *Steinernema*.

In both *Xenorhabdus* and *Photorhabdus,* nearly all analyzed SM-related genes were found to be down-regulated in the Δ*arcZ* mutant, in accordance with the impaired SM production (Figure 4a & b). This provides a chemical background that is devoid of natural products, which allows for isolation and identification of a desired compound due to the absence of compounds with similar retention times. Therefore, Δ*arcZ* mutants could offer a powerful tool for (over-) production and identification of previously undescribed natural products. As

a proof of concept, we conducted a promotor exchange in front of *gxpS* in both *X. szentirmaii* Δ*arcZ* and *X. szentirmaii* Δ*hfq* and compared GXP-C production after induction to the WT (Figure 4c). GXP-C production was found to be increased 90.4 (±4.7)-fold in *X. szentirmaii* Δ*arcZ*::pCEP_GxpS and increased 138.6 (±17.1)-fold in *X. szentirmaii* Δ*hfq*::pCEP_GxpS compared to the WT (Figure 4c). The striking increase in production, as well as the dramatically reduced chemical background in both strains, highlights the potential of exploiting this regulatory cascade for selective SM production in a strain well-suited for natural product detection. Recently, we showed that this strategy could be applied in a high-throughput manner for rapid screening of bioactivities[32]. The same strategy used here in a Δ*arcZ* strain, demonstrates an alternative route to activation, without the complex perturbations associated with deleting the major RNA chaperone in these bacteria. Interestingly, some comparisons between these mechanisms can be drawn in other SM-producing Enterobacteriaceae (Figure 1a). *Erwinia* is a genus of plant pathogenic bacteria that produce SMs, where Hfq and ArcZ have both been implicated in virulence[33], while HexA is a negative regulator of secondary metabolites in these bacteria[34]. Similar parallels can also be seen from *Serratia* [35–37] and *Pseudomonas* [38], two other prolific SM producers. Although further investigations will be required to ascertain whether these apparent similarities represent identical mechanisms, the conserved nature of ArcZ in other SM-producing Enterobacteriaceae could suggest that this strategy may yield fresh avenues for rapid investigation into SM biosynthesis in other taxa.

Online Methods

Bacterial culture conditions

All *Photorhabdus* and *Xenorhabdus* strains were grown in LB with shaking for at least 16 hours at 30°C. *E. coli* strains were grown in LB with shaking for at least 16 hours at 37°C. The medium was supplemented with chloramphenicol (34 μg/ml), ampicillin (100 μg/ml), rifampicin (50μg/ml) or kanamycin (50 μg/ml) when appropriate. Promotor exchange mutants were induced by adding L-arabinose (2%, v/v) to the cultures. All plasmids and strains used in this study are listed in Supplementary Table 13 & 14.

Nematode bioassays

All nematodes were cultivated in *Galleria mellonella* and collected on white traps as previously described. Nematode bioassays were also performed as described elsewhere[4].

Creation of transposon mutant library

For the transposon mutagenesis, the plasmid pSAM_Kan (containing the mariner transposon) was constructed using pSAM_BT[39] as a template. To do this, the plasmid was linearized using the primers NN191/NN192. The kanamycin resistance cassette was amplified from the pCOLA_ara_tacI plasmid using the primers NN193/NN194 introducing complementary overhangs to pSAM_BT at both ends of the PCR fragment. The kanamycin resistance cassette was fused with the linearized pSAM_BT plasmid using Hot Fusion cloning thereby replacing the erythromycin resistance cassette with kanamycin resistance. *E. coli* ST18 was transformed with the plasmid pSAM_Kan and further used for the creation of the transposon mutant library of *P. laumondii* TTO1 through conjugation. Transposon-

insertion mutants were selected on LB agar containing kanamycin. All primer sequences are listed in Supplementary Table 15.

Construction of mutant strains

For the deletion of the majority of ArcZ in *P. laumondii* TTO1, a 1123 bp upstream and a 1014 bp downstream product was amplified using the primers NN276/NN277 and NN278/NN279, respectively. The PCR products were fused using the complementary overhangs introduced by the primers and cloned into the *Pst*I and *Bgl*II linearized pEB17 plasmid. The resulting plasmid was used for transformation of *E. coli* s17-1 λ*pir*. Conjugation of the plasmid in *P. laumondii* strains and generation of deletion strains by homologous recombination through counter selection was done as previously described[40]. Deletion mutants were verified by PCR using the primers NN281/NN282 yielding a 632 bp fragment for mutants genetically equal to the WT and a 502 bp fragment for the desired deletion mutant. Complementation of the ArcZ deletion was achieved by inserting the full and intact version of ArcZ at the original locus. To do this, a 2207 bp PCR product was amplified using the primers NN276/NN279 including the upstream and downstream region required for homologous recombination and the full length ArcZ. The fragment was cloned into pEB17 as described above. The verified plasmid construct was used for transformation of *E. coli* s17-1 λ*pir* cells. The plasmid was transferred into *P. laumondii* Δ*arcZ* by conjugation and integrated into the genome of *P. laumondii* Δ*arcZ* by homologous recombination. The knock-in mutant was generated by a second homologous recombination through counter selection on LB plates containing 6% sucrose. Knock-in mutants were verified by PCR using the primers NN281/NN282 yielding a 632 bp fragment. The same strategy was used for the construction of the mutant strains in *X. szentirmaii*. To generate the promotor exchange mutants in front of *gxpS,* the plasmid pCEPKMR_ORF00346 was transferred into *X. szentirmaii* Δ*arcZ* and *X. szentirmaii* Δ*hfq* by conjugation and integrated into the genome by homologous recombination.

DNA extraction

Genomic DNA was extracted using the Gentra Puregene Yeast/Bact Kit (Qiagen) following the manufacturer's instructions. For sequencing of transposon-insertion mutants, genomic DNA was extracted using the DNeasy Blood & Tissue Kit (Qiagen).

DNA sequencing and identification of transposon insertion site

DNA isolated from the transposon-insertion mutants was sequenced on the Illumina NextSeq platform. DNA libraries were constructed using the Nextera XT DNA preparation kit (Illumina) and whole genome sequencing was performed using 2 x 150bp paired-end chemistry. A sequencing depth of >50× was targeted for each sample. Genomes were assembled with SPAdes (v 3.10.1)[41] and annotated with Prokka v 1.12[42]. Completed genome sequences were analysed and viewed in Geneious v 6 & 9.1 (https://www.geneious.com).

Europe PMC Funders Author Manuscripts

RNA extraction, sequencing and analysis

Pre-cultures of *P. laumondii* TTO1, *X. szentirmaii* DSM16338, and their respective ArcZ deletion and knock-in mutants were grown in LB broth overnight with shaking, at 30 °C. The following day, the pre-cultures were used to inoculate fresh LB at an OD_{600} of 0.3. Cells were grown to mid-exponential phase (OD values for each experiment can be found in Supplementary Table 3). RNA was extracted using the RNeasy Mini Kit (Qiagen) following the manufacturer's instructions. To facilitate cell lysis, the cells were pelleted and snap frozen in liquid nitrogen for 1 min after removing the supernatant. After thawing and resuspending in lysis buffer, the cells were vortexed for 30 sec before proceeding with the protocol. RNA for small RNA libraries were extracted in duplicate, during the mid-exponential phase for *P. laumondii* TTO1 and *X. szentirmaii*.

RNA was sequenced with 150bp paired-end sequencing by Novogene following rRNA depletion with a RiboZero kit and library preparation following the Illumina protocol for strand-specific libraries. Raw data was trimmed using Trimmomatic[43] and mapped to the reference genome downloaded from NCBI (NC_005126.1 for *P. laumondii* and NZ_NIBV00000000.1 for *X. szentirmaii*) using bowtie2 (v2.3.4.3)[44]. Resulting .sam files were converted to .bam files using samtools (v1.8) [45] and featureCounts (a part of the subread package) [46] was used to count reads mapping to annotated genes. Count files were then uploaded to degust (http://degust.erc.monash.edu/) and analyzed using the voom/limma method of normalization. Only genes with an absolute fold change >2 and false discovery rate < 0.01 were considered significantly regulated. Statistical analysis was performed in R (v 3.6.1) on the degust platform, where exact code is available to view.

Northern blot analysis

For Northern blot analysis, total RNA was prepared and analyzed as described previously[47]. Briefly, RNA samples were separated on 6% polyacrylamide / 7 M urea gels and transferred to Hybond–XL membranes (GE Healthcare) by electro-blotting. Membranes were hybridized in Roti-Hybri-Quick buffer (Roth) at 42°C with gene-specific [^{32}P] end-labeled DNA oligonucleotides, and washed in three subsequent steps with SSC (5x, 1x, 0.5x) / 0.1% SDS wash buffer. Signals were visualized on a Typhoon FLA 7000 phosphorimager (FUJIFILM). Oligonucleotides for Northern blot analyses are listed in Supplementary Table 15.

Compensatory base mutation and GFP fluorescence assay

Plasmids pMH078 and pMH079 were generated using Gibson assembly[48]. For plasmid pMH078 the *arcZ* gene was amplified using *P. laumondii* TTO1 genomic DNA with oligonucleotides KPO-6147 and KPO-6148 and fused into a pEVS143 vector backbone[49], linearized with KPO-0092 and KPO-1397. To construct plasmid pMH079, the 5'UTR and the first 20 aa of *hexA* were amplified using *P. laumondii* TTO1 genomic DNA with KPO-6145 and KPO-6146, and the pXG10-*gfp* vector[50] was linearized with KPO-1702 and KPO-1703. pMH078 and pMH079 served as templates to insert single point mutations in the *arcZ* gene as well as the *hexA* 5'UTR using site-directed mutagenesis and oligonucleotide combinations KPO-6156/KPO-6157 and KPO-6164/KPO-6165, respectively, yielding plasmids pMH080 and pMH081.

Target regulation using GFP reporter fusions was analyzed as described previously[50]. *E. coli* Top10 cells were grown overnight in LB medium (37°C, 200 rpm shaking conditions). Three independent cultures were used for each strain. Cells were washed in PBS and GFP fluorescence intensity was determined using a Spark 10 M plate reader (TECAN). Control samples not expressing fluorescence proteins were used to subtract background fluorescence.

CappableSeq analysis

Cappable seq was performed as previously described[51] by Vertis Biotechnologies (Germany). Raw sequences were trimmed with Trimmomatic[43] and mapped with bowtie2[44] to NC_005126.1 for *P. laumondii* and NZ_NIBV00000000.1 for *X. szentirmaii*. Transcriptional start sites were detected using readXplorer's (v2.2.3)[52] built in TSS detection function with the following settings: use only single perfect matches, minimum number of read starts = 100, minimum percent coverage increase = 750, detect previously undescribed transcripts, min. transcript extension = 40, max distance to feature of leaderless transcripts = 5, associate neighbouring TSS within 3bp.

RIP-seq analysis

Overnight cultures of *P. laumondii* TTO1 (WT and Hfq^{3xFLAG}) were inoculated into fresh LB media in duplicate and grown at 30 °C with shaking at 200 rpm. Bacteria were harvested by centrifugation at 4°C, 4000 rpm for 15 min when cells reached OD_{600}=0.5 and OD_{600}=5.0. Cell pellets were resuspended in 1 mL lysis buffer (20 mM Tris pH 8.0, 150 mM KCl, 1 mM MgCl2, 1 mM DTT) and pelleted again by centrifugation (5 min, 11,200 g, 4°C). The supernatants were discarded and the pellets were snap-frozen in liquid nitrogen. After thawing on ice, cells were resuspended in 800 µl lysis buffer and transferred into tubes containing 300 µl glass beads to break cells via a Bead Ruptor (150 sec, twice, 2 min break on ice in between). After short centrifugation (15,000 g, 4°C), lysates were transferred into fresh precooled tubes and centrifuged for 30 minutes at 15,200 g at 4°C. The cleared lysates were transferred into fresh tubes and incubated with 35 µl FLAG-antibody (Monoclonal ANTI-FLAG M2, Sigma, #F1804) with rotation for 45 min at 4°C, followed by addition of 75 µl Protein G Sepharose (Sigma, #P3296) and rotating for 45 min at 4°C again. After five wash steps with lysis buffer (via inverting the tube gently and centrifuging for 4 min at 4° C), samples were subjected to RNA and protein separation by Phenol:Chloroform:Isoamylalcohol (P:C:I; 25:24:1, pH 4.5, Roth) extraction. The upper phase (~ 500 µl) was transferred into to a fresh tube and precipitated overnight at −20°C with 1.5 ml EtOH:Na(acetate) (30:1) and 1.5 µl GlycoBlue (#AM9516, Ambion). After centrifugation for 30 minutes at 11,200 rpm at 4°C, RNA pellets were washed with 500 µl 70% EtOH, dried and resuspended in 15.5 µl nuclease-free H_2O. RNA was treated with 2 µl DNase I, 0.5 µl RNase inhibitor and 2 µl 10x DNase buffer at 37°C for 30 min. Afterwards, samples were supplemented with 100 µl H_2O, and again subjected to P:C:I extraction. The upper phase (~120 µl) was transferred into a fresh tube with addition of 2.5-3 volumes (~350 µl) of EtOH:Na(acetate) (30:1) and stored at −20°C overnight for RNA precipitation. RNA pellets were harvested via centrifugation for 30 min at 13,000 rpm, 4 °C, and washed with 500 µl 70% EtOH, dried and resuspended in nuclease-free H_2O. cDNA libraries were prepared using the NEBNext Small RNA Library Prep Set for Illumina (NEB, #E7300S)

according to the manufacturer's instructions and sequenced on a HiSeq 1500 system in single-read mode with 100 nt read length.

For RIPseq analysis, the enriched/control sample pairs were normalized by the number of raw reads present after trimming. Depth counts of all samples were obtained using samtools (v1.8)[45]. Only nucleotide positions with a depth of at least 50 reads in the enriched samples were taken for further analysis. The corresponding depth in the unenriched samples was matched for each nucleotide. A region was considered to be enriched if the enrichment factor was at least three and the corresponding 'enriched' nucleotide was present in both sample pairs. Finally, we considered a region to be enriched if more than five consecutive nucleotides were identified as enriched.

ArcZ binding prediction

ArcZ from *E. coli* was used to define the boundaries of ArcZ in *Xenorhabdus* and *Photorhabdus*. We then took our annotated ArcZ sequence together with several ArcZ homologs from other Enterobacteriaceae (listed in Supplementary Table 9) and used the online CopraRNA tool[22], a part of the Freiburg RNA tools suite[53], with default parameters.

Metabolite extraction and HPLC-MS/MS analysis

Fresh 10 ml of LB was inoculated with an overnight culture to an OD_{600} = 0.1. After 72 h of cultivation at 30°C with shaking, 1 ml of the culture was removed from the culture, centrifuged for 20 min at 13,300 rpm and the supernatant was directly subjected for HPLC-UV/MS analysis using a Dionex Ultimate 3000 system with a Bruker AmaZon X mass spectrometer. The compounds peak areas were quantified using TargetAnalysis 1.3 (Bruker). All analyzed compounds are listed in Supplementary Table 16.

Proteome analysis

The detail of the proteomics procedure was previously published.[54] In short, to extract proteins from *P. laumondii*, frozen cell pellets 300 µL lysis buffer (0.5% Na-desoxycholate in 100 mM NH_4HCO_3) were added to the cell pellet, and incubated at 95°C for 10 min. The protein concentration in the supernatant was determined with a BCA Protein Assay Kit (Thermo Fisher, #23252). Reduction and alkylation was performed at 95 °C using 5mM TCEP and 10mM Chloroacetamide for 15 min. 50 µg of protein was transferred to fresh reaction tubes and protein digestion was carried out overnight at 30 °C with 1 µg trypsin (Promega). After digest, the peptides were desalted using CHROMABOND Spincolumns (Macherey-Nagel) that were conditioned with 500 µL of acetonitrile and equilibrated with 500 µL and 150 µL 0.1% TFA. After loading the peptides were washed with 500 µL 0.1% TFA in 5:95 acetonitrile:water, peptides were eluted with 400 µL 0.1% TFA in 50:50 acetonitrile:water. Peptides were concentrated and dried under vacuum at 50°C and dissolved in 100 µL 0.1% TFA by 25 s of sonication and incubation at 22°C under shaking at 1200 rpm for 5 min. 1 µg peptide was analyzed using liquid chromatography-mass spectrometry (LC-MS/MS).

The LC-MS/MS analysis including lable-free quantification was carried out as previously described[54], with minor modifications.

Europe PMC Funders Author Manuscripts

LC-MS/MS analysis of protein digests was performed on Q-Exactive Plus mass spectrometer connected to an electrospray ion source (Thermo Fisher Scientific). Peptide separation was carried out using Ultimate 3000 nanoLC-system (Thermo Fisher Scientific), equipped with packed in-house C18 resin column (Magic C18 AQ 2.4 μm, Dr. Maisch). The peptides were first loaded onto a C18 precolumn (preconcentration set-up) and then eluted in backflush mode with a gradient from 98 % solvent A (0.15 % formic acid) and 2 % solvent B (99.85 % acetonitrile, 0.15 % formic acid) to 35 % solvent B over 30 min. Label-free quantification was done using Progenesis QI software (Nonlinear Dynamics, v2.0), MS/MS search was performed in MASCOT (v2.5, Matrix Science) against the Uniprot *Photorhabdus laumondii* protein database. The following search parameters were used: full tryptic search with two missed cleavage sites, 10ppm MS1 and 0.02 Da fragment ion tolerance. Carbamidomethylation (C) as fixed, oxidation (M) and deamidation (N,Q) as variable modification. Progenesis outputs were further processed with SafeQuant[55].

Europe PMC Funders Author Manuscripts

Extended Data

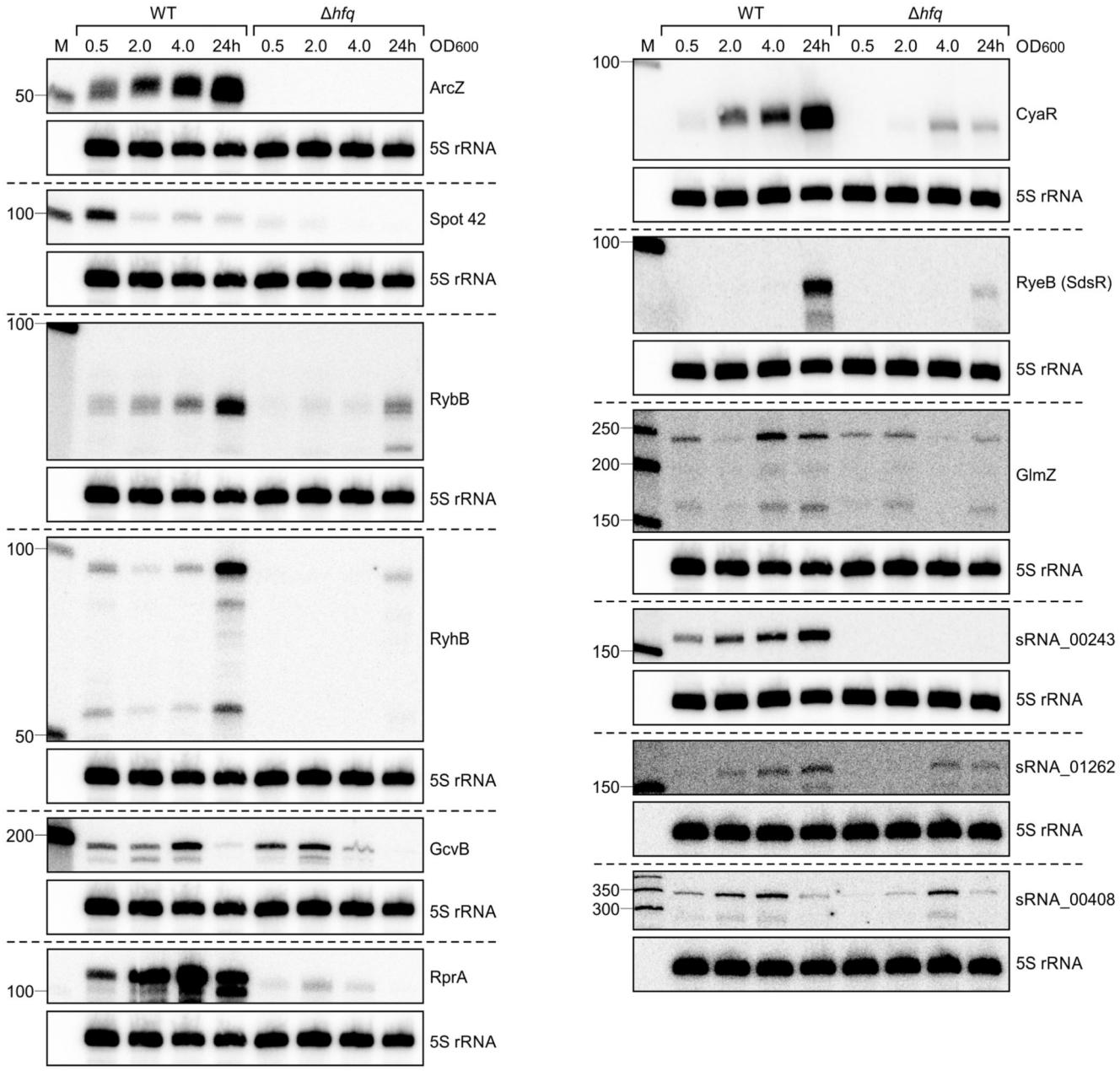

Extended Data Fig. 1.

Expression of various sRNAs in *P. laumondii* at different time points. RNA samples of *P. laumondii* WT and Δhfq strains were taken at three different OD600 values (0.5, 2 and 4) and after 24 h of growth. The RNA was loaded on Northern blots and probed for the indicated sRNAs. Probing for 5S rRNA served as loading control.

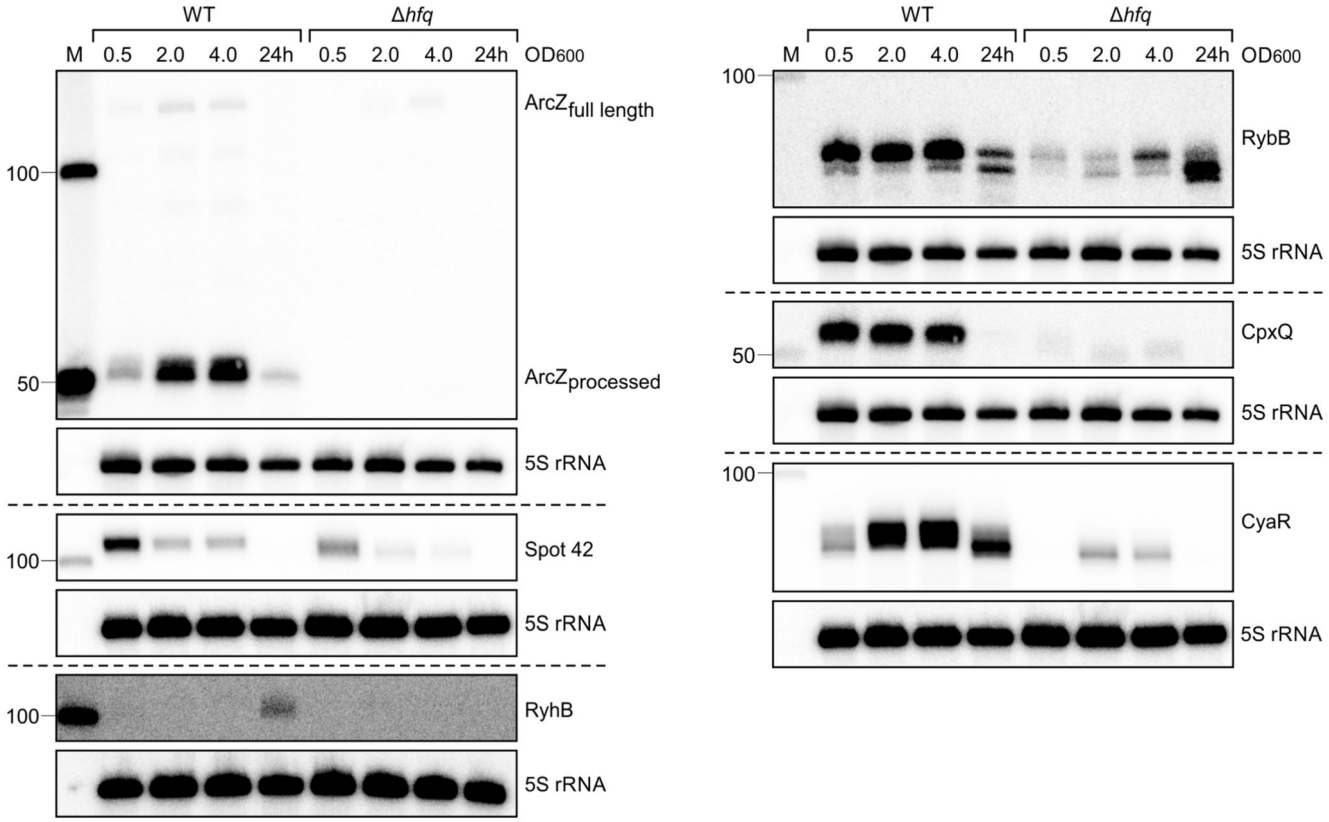

Extended Data Fig. 2.

Expression of various sRNAs in *X. szentirmaii* at different time points. RNA samples of *X. szentirmaii* WT and Δhfq strains were taken at three different OD600 values (0.5, 2 and 4) and after 24 h of growth. The RNA was loaded on Northern blots and probed for the respective sRNAs. Probing for 5S ribosomal RNA served as loading control.

Europe PMC Funders Author Manuscripts

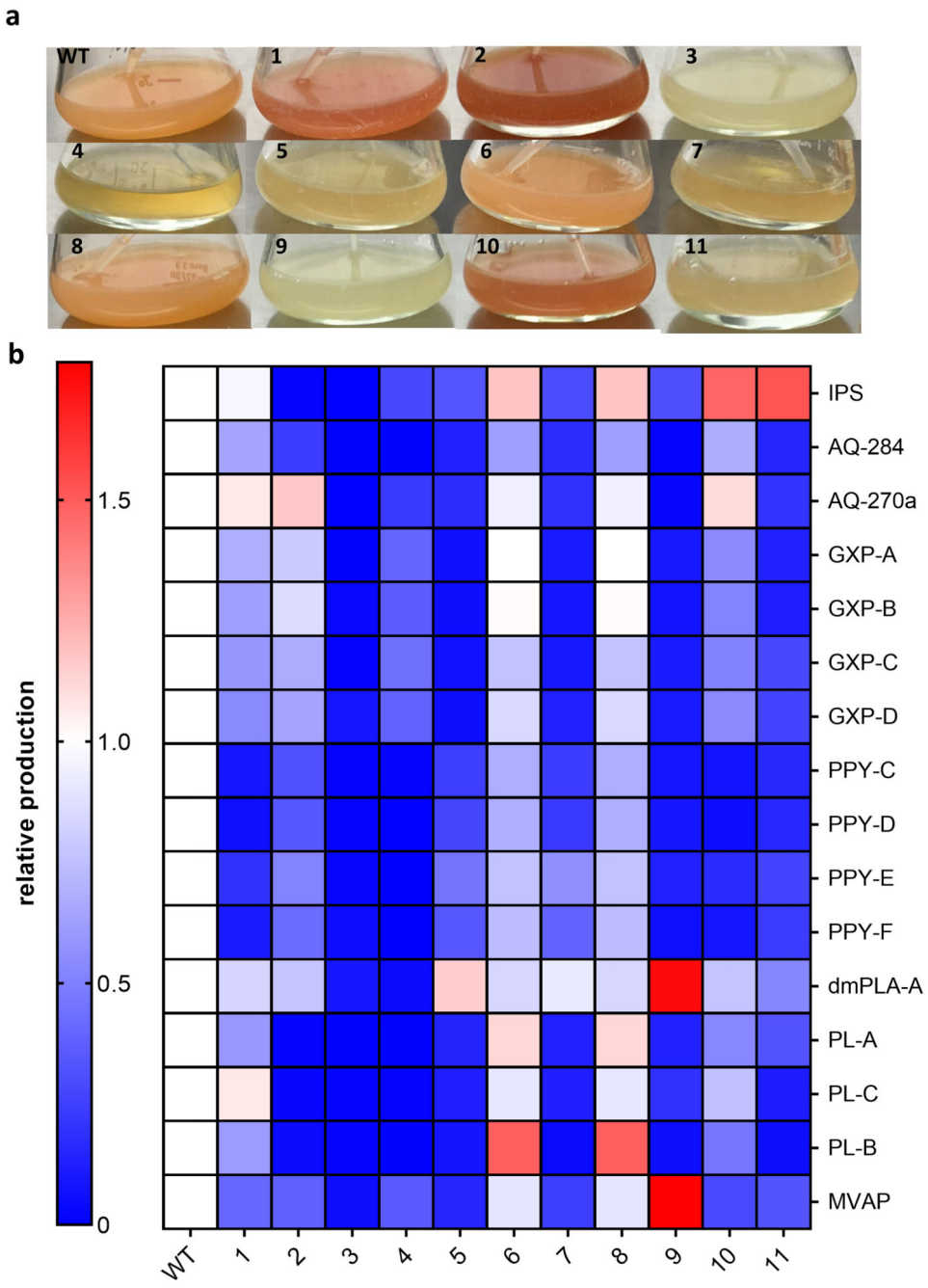

Extended Data Fig. 3.

Phenotype of transposon insertion mutants of *P. laumondii*. **a**. Differences in pigmentation of transposon insertion mutant liquid cultures compared to WT. Depicted are eleven transposon insertion mutants and a WT culture after 3 d of cultivation at 30°C with shaking. **b**. SM-profiles of the transposon insertion mutants. Relative SM production was quantified from duplicates using TargetAnalysis (Bruker) and compared to the WT of *P. laumondii* after 72 h cultivation at 30°C with shaking. Mutant 3 was analysed further and the transposon insertion was identified in the arcZ gene.

Europe PMC Funders Author Manuscripts

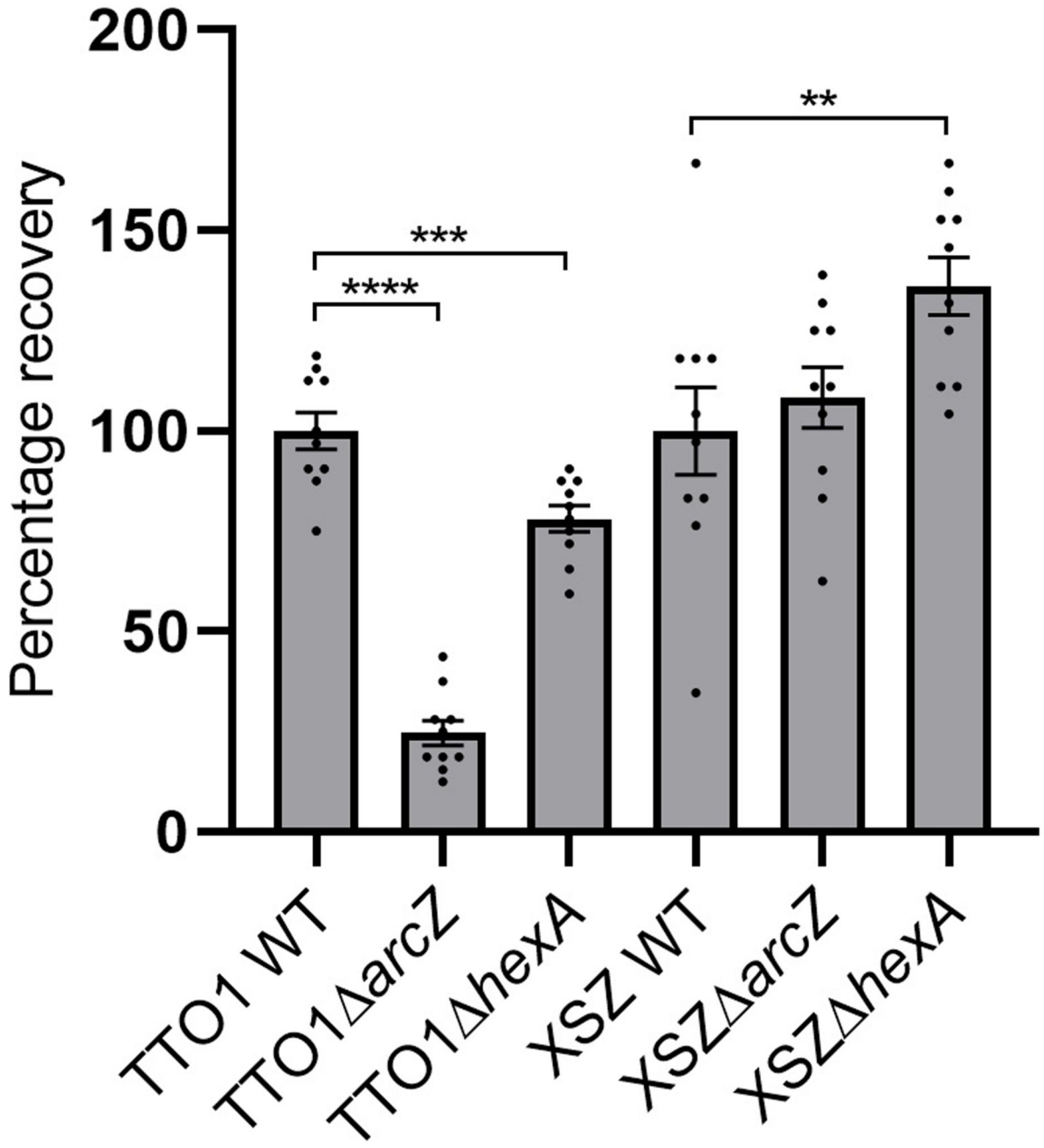

Extended Data Fig. 4.

Infective juvenile development to hermaphrodites with strains of *P. laumondii* and *X. szentirmaii*. Data are presented as mean values +/- SEM. Dots represent biologically independent replicates (n=10). Asterisks indicate statistical significance (* $p<0.05$, ** $p<0.005$, *** $p<0.0005$, **** $p<0.00005$) of relative recovery compared to WT recovery levels. Statistical significances were calculated using a two-sided unpaired t-test. Exact p values (left to right, respectively) for *P. laumondii* TTO1 correspond to p= <0.0001, 0.0006 and for *X. szentirmaii* to p= 0.56, 0.0094.

Supplementary Material

Refer to Web version on PubMed Central for supplementary material.

Acknowledgements

This work was funded in part by the DFG (SFB 902, Project B17) and the LOEWE Centre for Translational Biodiversity Genomics (TBG) supported by the State of Hesse. K.P. acknowledges funding by DFG (EXC 2051, Project 390713860), the Vallee Foundation, and the European Research Council (StG-758212). We thank Andrew Goodman for providing pSAM-BT and helpful discussions. We thank Laura Pöschel and Antje K. Heinrich for plasmid construction.

Data availability

All .mzXML files from HPLC-MS runs are available at MassIVE (https://massive.ucsd.edu) under the ID MSV000084163. Raw sequence data is available at the European nucleotide archive (https://www.ebi.ac.uk/ena/) under project accession numbers PRJEB33827 and PRJEB24159. The proteomic data can be accessed at PRIDE (https://www.ebi.ac.uk/pride/) with the project accession number PXD019095. Source Data are provided with this paper.

References

1. Stock SP, Campbell JF, Nadler SA. Phylogeny of Steinernema travassos, 1927 (Cephalobina: Steinernematidae) inferred from ribosomal DNA sequences and morphological characters. J Parasitol. 2001; 87:877–889. [PubMed: 11534654]
2. Forst S, Dowds B, Boemare N, Stackebrandt E. Xenorhabdus and Photorhabdus spp.: bugs that kill bugs. Annu Rev Microbiol. 1997; 51:47–72. [PubMed: 9343343]
3. Engel Y, Windhorst C, Lu X, Goodrich-Blair H, Bode HB. The Global Regulators Lrp, LeuO, and HexA Control Secondary Metabolism in Entomopathogenic Bacteria. Frontiers in Microbiology. 2017; 8:209. [PubMed: 28261170]
4. Tobias NJ, et al. Photorhabdus-nematode symbiosis is dependent on hfq-mediated regulation of secondary metabolites. Environ Microbiol. 2017; 19:119–129. [PubMed: 27555343]
5. Carrier M-C, Lalaouna D, Massé E. Broadening the Definition of Bacterial Small RNAs: Characteristics and Mechanisms of Action. Annu Rev Microbiol. 2018; 72:141–161. [PubMed: 30200848]
6. Vogel J, Luisi BF. Hfq and its constellation of RNA. Nat Rev Microbiol. 2011; 9:578–589. [PubMed: 21760622]
7. Santiago-Frangos A, Woodson SA. Hfq chaperone brings speed dating to bacterial sRNA. Wiley Interdiscip Rev RNA. 2018; 9 e1475 [PubMed: 29633565]
8. Chao Y, Papenfort K, Reinhardt R, Sharma CM, Vogel J. An atlas of Hfq-bound transcripts reveals 3' UTRs as a genomic reservoir of regulatory small RNAs. EMBO J. 2012; 31:4005–4019. [PubMed: 22922465]
9. Papenfort K, et al. Specific and pleiotropic patterns of mRNA regulation by ArcZ, a conserved, Hfq-dependent small RNA. Mol Microbiol. 2009; 74:139–158. [PubMed: 19732340]
10. Mandin, Gottesman S. Integrating anaerobic/aerobic sensing and the general stress response through the ArcZ small RNA. EMBO J. 2010; 29:3094–3107. [PubMed: 20683441]
11. Chao Y, et al. In Vivo Cleavage Map Illuminates the Central Role of RNase E in Coding and Non-coding RNA Pathways. Mol Cell. 2017; 65:39–51. [PubMed: 28061332]
12. Beemelmanns C, Guo H, Rischer M, Poulsen M. Natural products from microbes associated with insects. Beilstein J Org Chem. 2016; 12:314–327. [PubMed: 26977191]
13. Shi Y-M, Bode HB. Chemical language and warfare of bacterial natural products in bacteria-nematode-insect interactions. Nat Prod Rep. 2018; 35:309–335. [PubMed: 29359226]

14. Brachmann AO, et al. Pyrones as bacterial signaling molecules. Nat Chem Biol. 2013; 9:573–578. [PubMed: 23851573]
15. Brameyer S, Kresovic D, Bode HB, Heermann R. Dialkylresorcinols as bacterial signaling molecules. Proc Natl Acad Sci USA. 2015; 112:572–577. [PubMed: 25550519]
16. Joyce SA, et al. Bacterial biosynthesis of a multipotent stilbene. Angew Chem Int Ed Engl. 2008; 47:1942–1945. [PubMed: 18236486]
17. Cai X, et al. Entomopathogenic bacteria use multiple mechanisms for bioactive peptide library design. Nat Chem. 2017; 9:379–386. [PubMed: 28338679]
18. Crawford JM, Portmann C, Zhang X, Roeffaers MBJ, Clardy J. Small molecule perimeter defense in entomopathogenic bacteria. Proc Natl Acad Sci USA. 2012; 109:10821–10826. [PubMed: 22711807]
19. Theodore CM, King JB, You J, Cichewicz RH. Production of cytotoxic glidobactins/luminmycins by Photorhabdus asymbiotica in liquid media and live crickets. J Nat Prod. 2012; 75:2007–2011. [PubMed: 23095088]
20. Lango-Scholey L, Brachmann AO, Bode HB, Clarke DJ. The expression of stlA in Photorhabdus luminescens is controlled by nutrient limitation. PLoS ONE. 2013; 8 e82152 [PubMed: 24278476]
21. Kontnik R, Crawford JM, Clardy J. Exploiting a global regulator for small molecule discovery in Photorhabdus luminescens. ACS Chem Biol. 2010; 5:659–665. [PubMed: 20524642]
22. Wright PR, et al. CopraRNA and IntaRNA: predicting small RNA targets, networks and interaction domains. Nucleic Acids Res. 2014; 42:W119–23. [PubMed: 24838564]
23. Joyce SA, Clarke DJ. A hexA homologue from Photorhabdus regulates pathogenicity, symbiosis and phenotypic variation. Mol Microbiol. 2003; 47:1445–1457. [PubMed: 12603747]
24. Bouvier M, Sharma CM, Mika F, Nierhaus KH, Vogel J. Small RNA binding to 5' mRNA coding region inhibits translational initiation. Mol Cell. 2008; 32:827–837. [PubMed: 19111662]
25. Sharma CM, Darfeuille F, Plantinga TH, Vogel J. A small RNA regulates multiple ABC transporter mRNAs by targeting C/A-rich elements inside and upstream of ribosome-binding sites. Genes Dev. 2007; 21:2804–2817. [PubMed: 17974919]
26. Yang Q, Figueroa-Bossi N, Bossi L. Translation enhancing ACA motifs and their silencing by a bacterial small regulatory RNA. PLoS Genet. 2014; 10 e1004026 [PubMed: 24391513]
27. Wenger RH. Mammalian oxygen sensing, signalling and gene regulation. J Exp Biol. 2000; 203:1253–1263. [PubMed: 10729275]
28. Chen JJ, London IM. Regulation of protein synthesis by heme-regulated eIF-2 alpha kinase. Trends BioChem Sci. 1995; 20:105–108. [PubMed: 7709427]
29. Qi Z, Hamza I, O'Brian MR. Heme is an effector molecule for iron-dependent degradation of the bacterial iron response regulator (Irr) protein. Proc Natl Acad Sci USA. 1999; 96:13056–13061. [PubMed: 10557272]
30. Rao AU, Carta LK, Lesuisse E, Hamza I. Lack of heme synthesis in a free-living eukaryote. Proc Natl Acad Sci USA. 2005; 102:4270–4275. [PubMed: 15767563]
31. Bolla R. Developmental nutrition of nematodes: the biochemical role of sterols, heme compounds, and lysosomal enzymes. J Nematol. 1979; 11:250–259. [PubMed: 19300643]
32. Bode E, et al. Promoter Activation in Δhfq Mutants as an Efficient Tool for Specialized Metabolite Production Enabling Direct Bioactivity Testing. Angew Chem Int Ed Engl. 2019; 58:18957–18963. [PubMed: 31693786]
33. Zeng Q, McNally RR, Sundin GW. Global Small RNA Chaperone Hfq and Regulatory Small RNAs Are Important Virulence Regulators in Erwinia amylovora. J Bacteriol. 2013; 195:1706–1717. [PubMed: 23378513]
34. Mukherjee A, Cui Y, Ma W, Liu Y, Chatterjee AK. hexA of Erwinia carotovora ssp. carotovora strain Ecc71 negatively regulates production of RpoS and rsmB RNA, a global regulator of extracellular proteins, plant virulence and the quorum-sensing signal, N-(3-oxohexanoyl)-l-homoserine lactone. Environ Microbiol. 2000; 2:203–215. [PubMed: 11220306]
35. Matilla MA, Leeper Salmond FJ, George PC. Biosynthesis of the antifungal haterumalide, oocydin A, in Serratia, and its regulation by quorum sensing, RpoS and Hfq. Environ Microbiol. 2015; 17:2993–3008. [PubMed: 25753587]

36. Wilf Salmond NM, George PC. The stationary phase sigma factor, RpoS, regulates the production of a carbapenem antibiotic, a bioactive prodigiosin and virulence in the enterobacterial pathogen Serratia sp ATCC 39006. Microbiology (Reading, Engl). 2012; 158:648–658.
37. Wilf NM, et al. The RNA chaperone, Hfq, controls two luxR-type regulators and plays a key role in pathogenesis and production of antibiotics in Serratia sp ATCC 39006. Environ Microbiol. 2011; 13:2649–2666. [PubMed: 21824244]
38. Shanks RMQ, et al. Suppressor analysis of eepR mutant defects reveals coordinate regulation of secondary metabolites and serralysin biosynthesis by EepR and HexS. Microbiology (Reading, Engl). 2017; 163:280–288.
39. Goodman AL, et al. Identifying genetic determinants needed to establish a human gut symbiont in its habitat. Cell Host Microbe. 2009; 6:279–289. [PubMed: 19748469]
40. Brachmann AO, et al. A type II polyketide synthase is responsible for anthraquinone biosynthesis in Photorhabdus luminescens. Chembiochem. 2007; 8:1721–1728. [PubMed: 17722122]
41. Bankevich A, et al. SPAdes: A New Genome Assembly Algorithm and Its Applications to Single-Cell Sequencing. J Comput Biol. 2012; 19:455–477. [PubMed: 22506599]
42. Seemann T. Prokka: rapid prokaryotic genome annotation. Bioinformatics. 2014; 30:2068–2069. [PubMed: 24642063]
43. Bolger AM, Lohse M, Usadel B. Trimmomatic: a flexible trimmer for Illumina sequence data. Bioinformatics. 2014; 30:2114–2120. [PubMed: 24695404]
44. Langmead B, Salzberg SL. Fast gapped-read alignment with Bowtie 2. Nat Methods. 2012; 9:357–359. [PubMed: 22388286]
45. Li H, et al. The Sequence Alignment/Map format and SAMtools. Bioinformatics. 2009; 25:2078–2079. [PubMed: 19505943]
46. Liao Y, Smyth GK, Shi W. featureCounts: an efficient general purpose program for assigning sequence reads to genomic features. Bioinformatics. 2014; 30:923–930. [PubMed: 24227677]
47. Fröhlich KS, Haneke K, Papenfort K, Vogel J. The target spectrum of SdsR small RNA in Salmonella. Nucleic Acids Res. 2016; 44:10406–10422. [PubMed: 27407104]
48. Gibson DG. Synthesis of DNA fragments in yeast by one-step assembly of overlapping oligonucleotides. Nucleic Acids Res. 2009; 37:6984–6990. [PubMed: 19745056]
49. Dunn AK, Millikan DS, Adin DM, Bose JL, Stabb EV. New rfp- and pES213-derived tools for analyzing symbiotic Vibrio fischeri reveal patterns of infection and lux expression in situ. Appl Environ Microbiol. 2006; 72:802–810. [PubMed: 16391121]
50. Corcoran CP, et al. Superfolder GFP reporters validate diverse new mRNA targets of the classic porin regulator, MicF RNA. Mol Microbiol. 2012; 84:428–445. [PubMed: 22458297]
51. Tobias NJ, Linck A, Bode HB. Natural Product Diversification Mediated by Alternative Transcriptional Starting. Angew Chem Int Ed Engl. 2018; 57:5699–5702. [PubMed: 29508935]
52. Hilker R, et al. ReadXplorer 2-detailed read mapping analysis and visualization from one single source. Bioinformatics. 2016; 32:3702–3708. [PubMed: 27540267]
53. Smith C, Heyne S, Richter AS, Will S, Backofen R. Freiburg RNA Tools: a web server integrating INTARNA, EXPARNA and LOCARNA. Nucleic Acids Res. 2010; 38:W373–7. [PubMed: 20444875]
54. Hakobyan A, Liesack W, Glatter T. Crude-MS Strategy for in-Depth Proteome Analysis of the Methane-Oxidizing Methylocystis sp. strain SC2. J Proteome Res. 2018; 17:3086–3103. [PubMed: 30019905]
55. Glatter T, et al. Large-scale quantitative assessment of different in-solution protein digestion protocols reveals superior cleavage efficiency of tandem Lys-C/trypsin proteolysis over trypsin digestion. J Proteome Res. 2012; 11:5145–5156. [PubMed: 23017020]
56. Tobias NJ, et al. Cyclo(tetrahydroxybutyrate) production is sufficient to distinguish between Xenorhabdus and Photorhabdus isolates in Thailand. Environ Microbiol. 2019; 121:303.

Europe PMC Funders Author Manuscripts

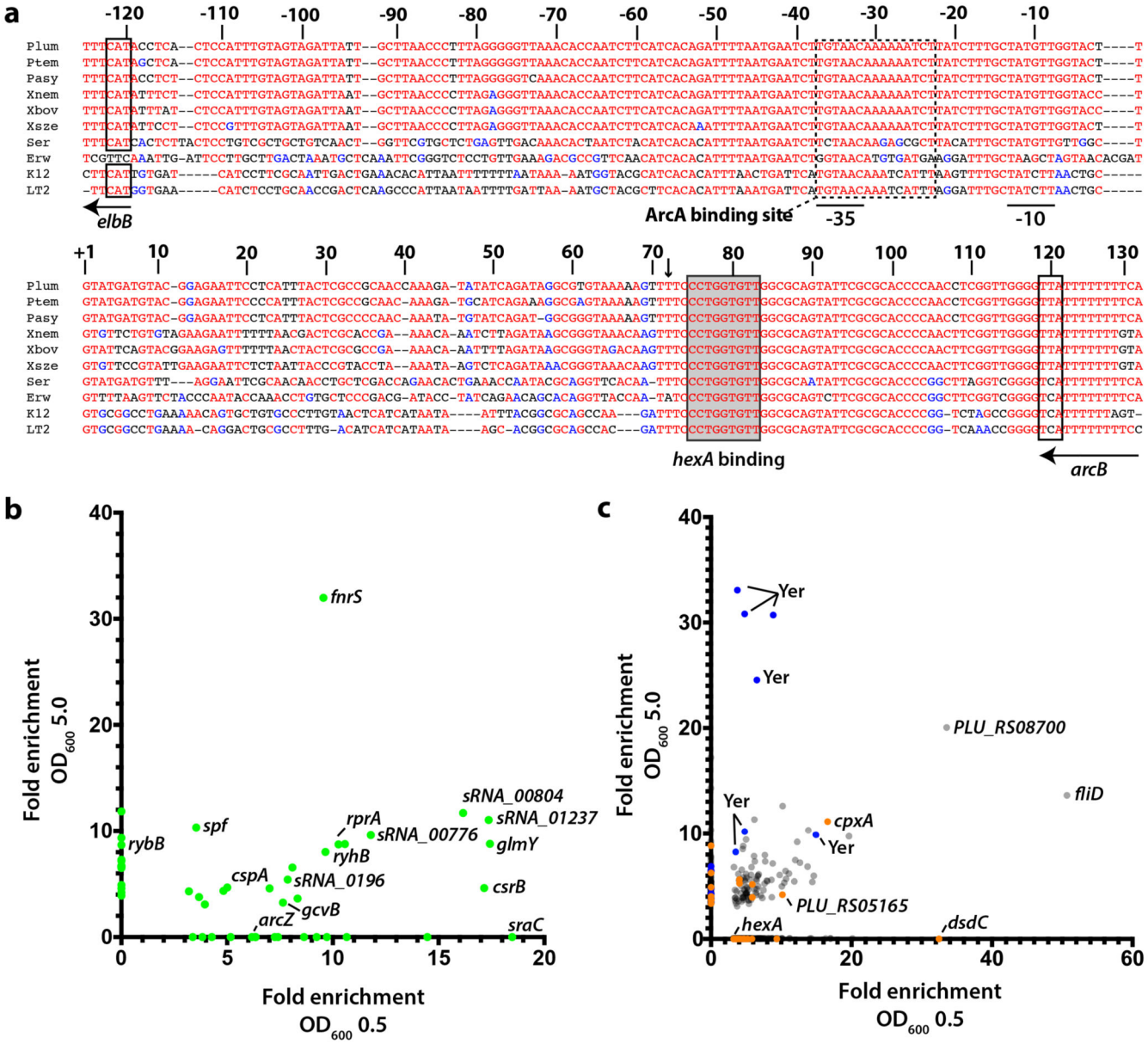

Figure 1a.

Alignment of *arcZ* sequences from *P. laumondii* TTO1, *P. temperata*, *P. asymbiotica*, *X. nematophila*, *X. bovienii*, *X. szentirmaii*, *Serratia marcescens*, *Erwinia amylovora*, *E. coli* K12 and *Salmonella typhimurium* LT2. Numbers refer to *P. laumondii* sequence. The +1 indicates the transcriptional start of the 129 nt *arcZ* sequence. Indicated are the start codon of *elbB* and the stop codon of *arcB*, -10 and -35 binding regions, as well as the conserved ArcA binding region[10] and the region of base-pairing to *hexA*. The site of ArcZ cleavage is indicated by an arrow. **b**. RIPseq enrichment in regions of sRNAs and **c**. mRNAs in a strain containing Hfq^{3xFLAG} when compared to the untagged control strain at both optical densities. For a complete list of enriched regions see Supplementary Tables 4 and 5. Blue

dots represent SM-related mRNAs, while orange dots represent mRNAs associated with annotated regulators.

Europe PMC Funders Author Manuscripts

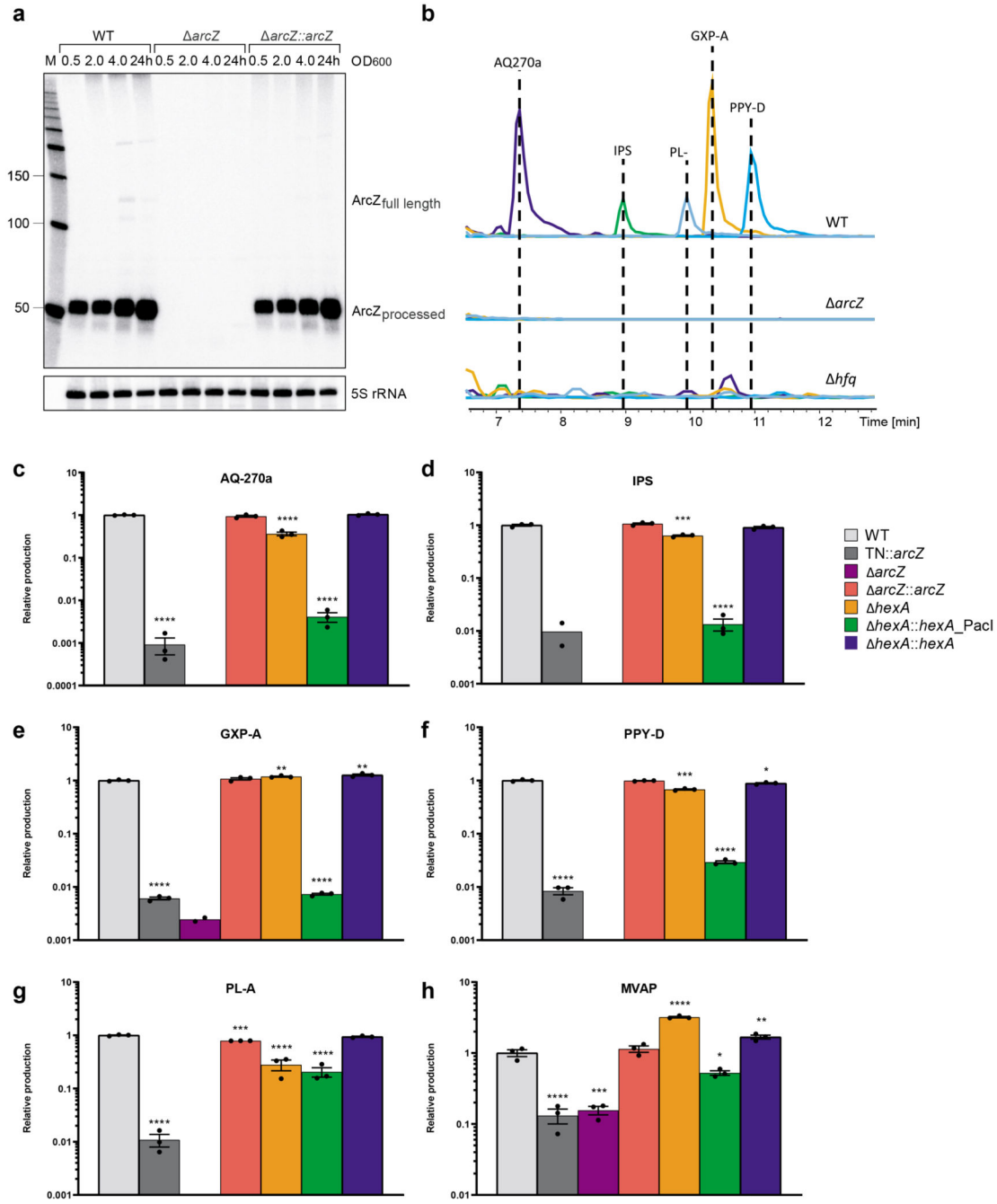

Figure 2a.

ArcZ expression in *P. laumondii* WT, Δ*arcZ* and Δ*arcZ*::*arcZ* cells detected by Northern blot analysis. Total RNA samples were collected at three different OD_{600} values (0.5; 2 and 4) and after 24 h of growth. Probing for 5S rRNA served as loading control. Representative blot image of two biologically independent replicates. **b**. Comparison of relative production titers of the major SMs produced by *P. laumondii* WT, Δ*arcZ* and Δ*hfq*. Depicted are the extracted ion chromatograms of anthraquinone (AQ-270a), isopropylstilbene (IPS), phurealipid A (PL-A), GameXPeptide A (GXP-A) and photopyrone D (PPY-D) in the WT and the mutant

Europe PMC Funders Author Manuscripts

strains. **c**-**h**. HPLC-MS quantification of **c**. AQ-270a, **d**. IPS, **e**. GXP-A, **f**. PPY-D, **g**. PL-A and **h**. MVAP in *P. laumondii* WT (light grey), TN::*arcZ* (grey), Δ*arcZ* (purple), Δ*arcZ*::*arcZ* (red), Δ*hexA* (orange), Δ*hexA*::*hexA*_PacI, (green) and Δ*hexA*::*hexA* (blue). All bars represent relative production in comparison to the wild type. Data are presented as mean values +/- SEM. Dots represent biologically independent replicates (n=3). Asterisks indicate statistical significance (* p<0.05, ** p<0.005, *** p<0.0005, **** p<0.0001) of relative production compared to WT production levels. For panels c to h statistical significances were calculated using a two-sided unpaired t-test. Exact p values (left to right, respectively) correspond to p= n.d. (not determined), n.d., 0.24, 0.0005, <0.0001, 0.12 in panel c; <0.0001, n.d., 0.20, <0.0001, <0.0001, 0.24 in panel d; <0.0001, n.d., 0.18, 0.0018, <0.0001, 0.0037 in panel e; <0.0001, n.d., 0.56, 0.0003, <0.0001, 0.013 in panel f; <0.0001, n.d., 0.0001, <0.0001, <0.0001, 0.059 in panel g; 0.0006, 0.0008, 0.34, <0.0001, 0.011, 0.0058 in panel g. Details of all analyzed compounds can be found in Supplementary Table 16.

Europe PMC Funders Author Manuscripts

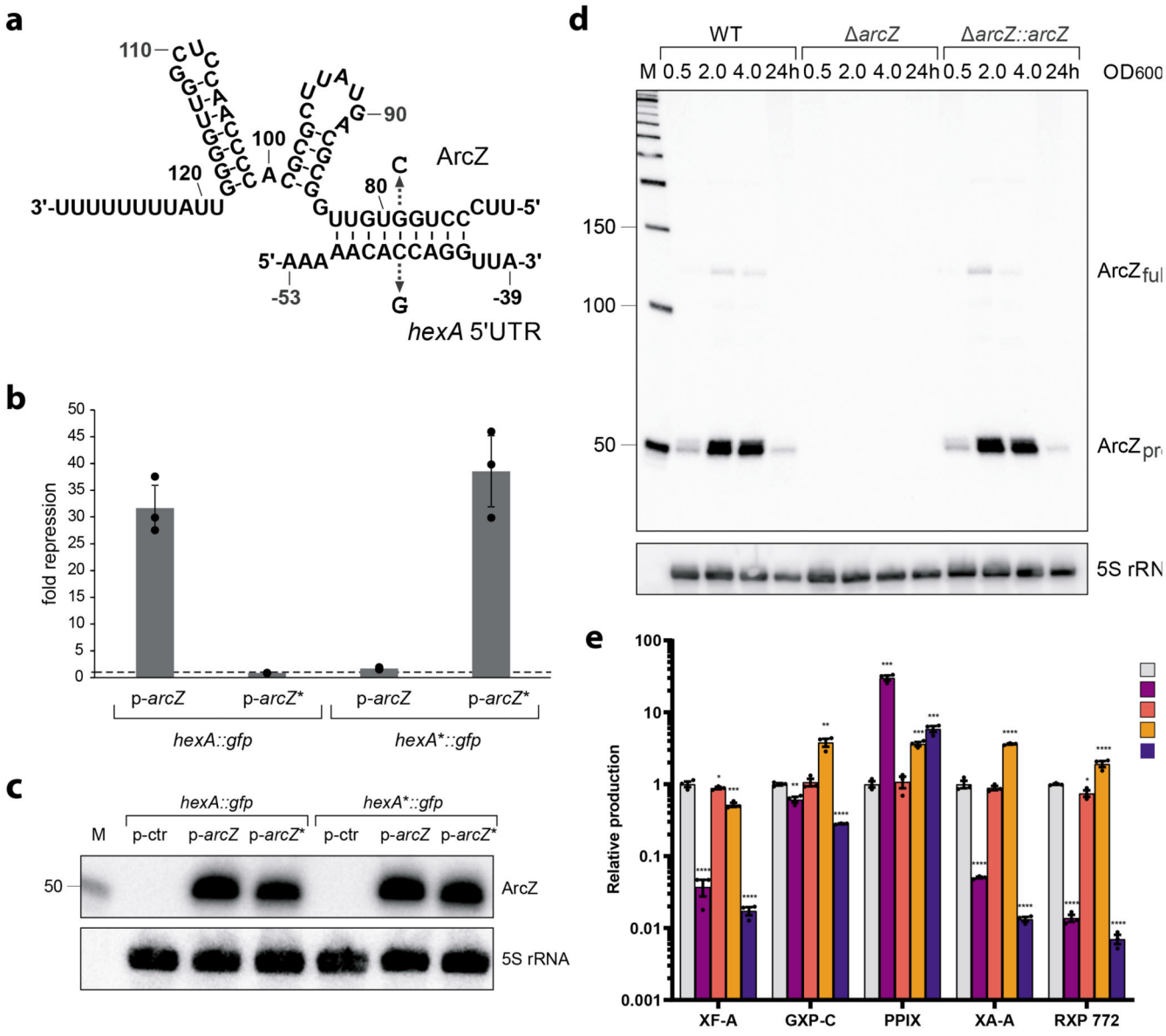

Figure 3a.

Predicted base-pairing interaction of ArcZ with the 5'-UTR of the *hexA* mRNA. Arrows indicate the single nucleotide mutations tested in b. **b**. Measurement of GFP signals derived from co-expression of a plasmid harbouring the 5'-UTR of *hexA* fused to *gfp* (*hexA::gfp*) or the same fusion with a single point mutation (C-46G, *hexA*:gfp*) with p-ctr, p-*arcZ* or p-*arcZ** (G79C). GFP levels of strains carrying the control plasmid (p-ctr) were set to 1. Data are presented as mean values +/- SD. Dots represent biologically independent replicates (n=3). **c**. Northern blot analysis of ArcZ expression corresponding to the GFP expression assay shown in b. 5S rRNA served as loading control. **d**. ArcZ expression in *X. szentirmaii* WT, Δ*arcZ* and Δ*arcZ*::*arcZ* cells detected by Northern blot analysis. Total RNA samples were collected at three different OD_{600} values (0.5; 2 and 4) and after 24 h of growth. 5S rRNA served as loading control. **e**. HPLC-MS quantification of strains of *X. szentirmaii* WT

Europe PMC Funders Author Manuscripts

(light grey), Δ*arcZ* (purple), Δ*arcZ*::*arcZ* (red), Δ*hexA* (orange) and Δ*hfq* (blue). Shown is the relative production of xenofuranone A (XF-A), GameXPeptide C (GXP-C), protoporphyrin IX (PPIX), xenoamicin A (XA-A) and rhabdopeptide 772 (RXP 772). See also Supplementary Table 16. Data are presented as mean values +/- SEM. Dots represent biologically independent replicates (n=3). Asterisks indicate statistical significance (* $p<0.05$, ** $p<0.005$, *** $p<0.0005$, **** $p<0.0001$) of relative production compared to WT production levels. For panel e statistical significances were calculated using a two-sided unpaired t-test. Exact p values (left to right, respectively) correspond to p= <0.0001, 0.021, 0.0001, <0.0001 for XF-A, 0.0034, 0.059, 0.0021, <0.0001 for GXP-C, 0.0001, 0.8, 0.0008, 0.0007 for PPIX, <0.0001, 0.14, <0.0001, <0.0001 for XA-A and <0.0001, 0.02, 0.0041, <0.0001 for RXP 772. Details of all analyzed compounds can be found in Supplementary Table 16.

Europe PMC Funders Author Manuscripts

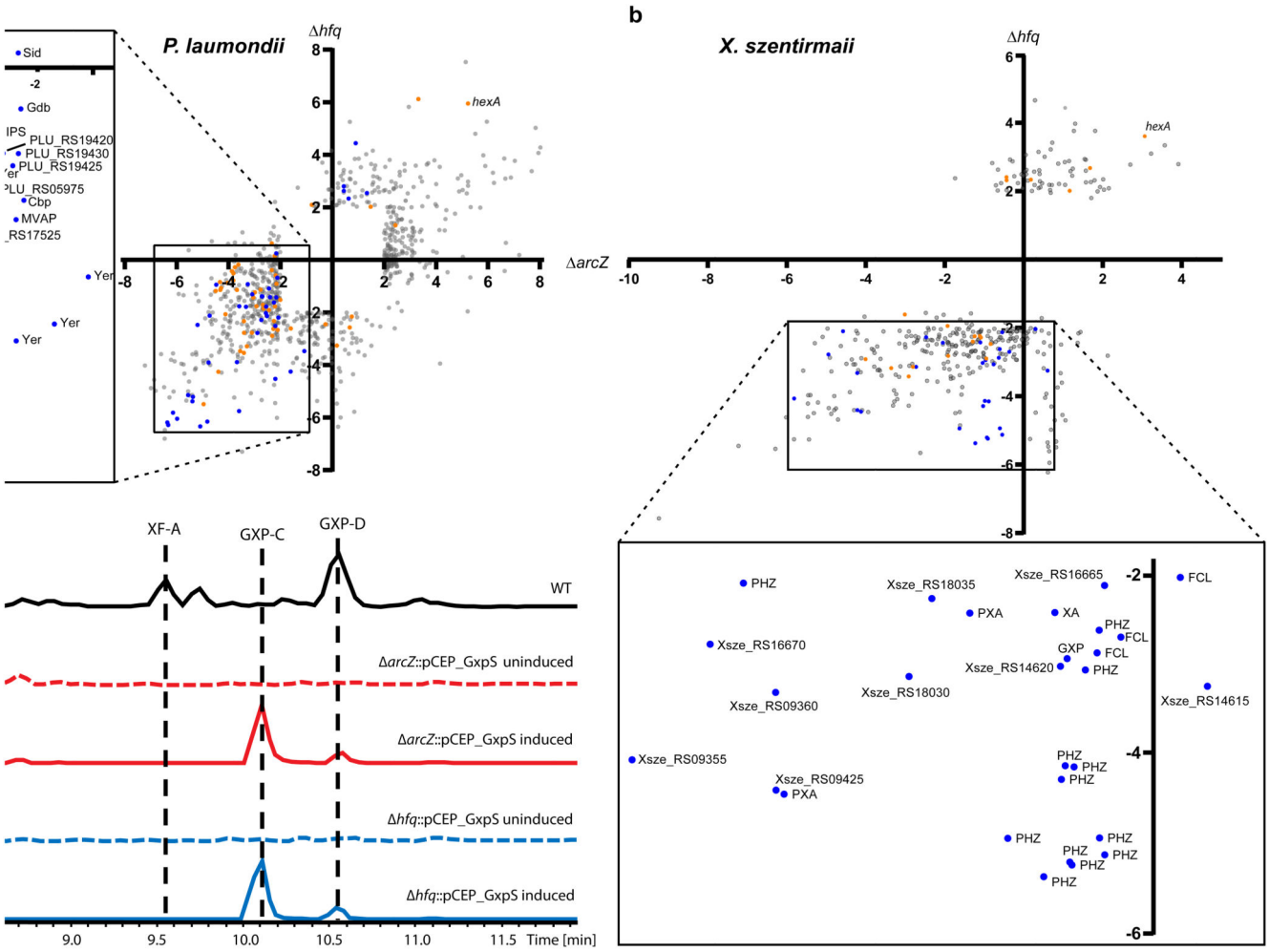

Figure 4.

Comparison of ArcZ and Hfq regulon **a**. *P. laumondii* and **b**. *X. szentirmaii*. Scatterplots show individual coding sequences and their corresponding regulatory changes compared to wild type in either the Δ*arcZ* (x-axis) or Δ*hfq* (y-axis) mutants, with SMs (blue dots) and regulators (orange dots) highlighted. The inset shows only SM-related coding sequences, including those associated with anthraquinone (AQ), mevalagmapeptide (MVAP), carbapenem (Cbp), yersiniabactin (YER), GameXPeptide (GXP), siderophore (SID), isopropylstilbene (IPS) and glidobactin (Gdb), phenazine (PHZ), fabclavine (FCL), xenoamicin (XA) and pyrrolizixenamide (PXA). **C** Base peak chromatograms (BPCs) of *X. szentirmaii* WT (black), Δ*arcZ*::pCEP_GxpS uninduced (red dotted line), Δ*arcZ*::pCEP_GxpS induced (red solid line), Δ*hfq*::pCEP_GxpS uninduced (blue dotted line) and Δ*hfq*::pCEP_GxpS induced (blue solid line). Peaks corresponding to (cyclo)tetrahydroxybutyrate (THB[56]), Linear GameXPeptide C (GXP-C), rhabdopeptide 772 (RXP), xenofuranone A (XF-A), as well as cyclic GXP-C and GXP-D. Five times zoom was applied to base peak chromatograms in the uninduced and wild type samples.

Europe PMC Funders Author Manuscripts